Correction of motion artifacts and scanning beam distortions in 3D ophthalmic optical coherence tomography imaging

Robert J. Zawadzki*[a], Alfred R. Fuller[b], Stacey S. Choi[a], David F. Wiley[b,c],
Bernd Hamann[b,c] and John S. Werner[a]

[a] Vision Science and Advanced Retinal Imaging Laboratory (VSRI), Dept. of Ophthalmology & Vision Science, UC Davis, 4860 Y Street, Suite 2400, Sacramento, CA, USA 95817;

[b] Visualization and Computer Graphics Research Group, Institute for Data Analysis and Visualization (IDAV), UC Davis, One Shields Avenue, Davis, CA 95616;

[c] Stratovan Corporation, Woodland, CA

ABSTRACT

The ability to obtain true three-dimensional (3D) morphology of the retinal structures is essential for future clinical and experimental studies. It becomes especially critical if the measurements acquired with different instruments need to be compared, or precise volumetric data are needed for monitoring and treatment of retinal disease. On the other hand, it is well understood that optical coherence tomography (OCT) images are distorted by several factors. Only limited work has been performed to eliminate these problems in ophthalmic retinal imaging, perhaps because they are less evident in the more common 2D representation mode of time-domain OCT. With recent progress in imaging speed of Fourier domain - OCT (Fd-OCT) techniques, however, 3D OCT imaging is more frequently being used, thereby exposing problems that have been ignored previously. In this paper we propose possible solutions to minimize and compensate for artifacts caused by subject eye and head motion, and distortions caused by the geometry of the scanning optics. The first is corrected by cross-correlation based B-scan registration techniques; the second is corrected by incorporating the geometry of the scanning beam into custom volume rendering software. Retinal volumes of optical nerve head (ONH) and foveal regions of healthy volunteer, with and without corrections, are presented. Finally, some common factors that may lead to increased distortions of the ophthalmic OCT image such as refractive error or position of the subject's head are discussed.

Keywords: (110.4500) Optical coherence tomography; (170.0110) Imaging system; (170.4470) Ophthalmology; (120.3890) Medical optics instrumentation

1. INTRODUCTION

Due to the latest developments in OCT [1-2], including its Fourier-domain extension [3-5] and commercialization, it has become an increasingly important tool for in vivo imaging of the retina in clinical settings. Acquisition speed of current FD-OCT systems allows measurements of volumetric retinal structures within 2 to 10 seconds, depending on the system's speed and lateral sampling density. Therefore volumetric representation of the retina, as in other medical areas, is becoming an increasingly important tool for ophthalmic clinical diagnosis and research. In this context it is important to remember that optical coherence tomography (OCT) images are distorted by several factors including geometry of the OCT scanning beam as well as head and eye motion. Only limited work has evaluated appropriate distortion correction [6-7]. In this paper we propose methods allowing correction of both motion and scanning beam distortions resulting in corrected volume of the retina. Scanning beam distortion correction algorithm presented in this paper is a part of our custom volumetric visualization software and is designed to take into account the actual geometry of the scanning optics of the OCT system used. To make it possible we defined 5 characteristic parameters that are specific for each OCT system, therefore allowing corrections of deformations introduced by this instrument.

*rjzawadzki@ucdavis.edu; phone: 1-916-734-5839; fax: 1-916-734-4543; web: http://vsri.ucdavis.edu

The results of this correction are immediately visualized by our custom 3D volume rendering software. We think that this "true" three-dimensional (3D) morphology of the retina may find its application in temporal monitoring of retinal disease as well as for comparisons across OCT platforms.

2. MATERIALS AND METHODS

The volumetric retinal data presented in this paper have been acquired by our clinical Fd-OCT system developed at UC Davis with collaboration with Duke University. More than 200 subjects, with healthy and diseased eyes, have been imaged with this system. This paper focuses on the correction of image distortion, thus only two representative retinal volumes acquired for the same subject over 6x6mm centered on foveal and ONH regions will be presented. Both volumes have passed our standard test of qualifying retinal volumes for volumetric reconstruction. This test includes estimating volume distortions by viewing movies showing all consecutive B-scans acquired in the volume as well as C-scans reconstructed from OCT images.

2.1. Experimental system

The experimental Fd-OCT system used for acquiring 3D volumes is shown in Figure 1, and described in detail elsewhere [8]. For experiments described here, we used a superluminescent diode (855@75nm) from Superlum allowing 4.5 μm axial resolution of the retina (n=1.38). Measured power at the subject's eye was equal to 700 μW. With our current spectrometer design, the maximum axial range (seen after the Fourier transform) is 2.7 mm in free space and around 2 mm in the eye.
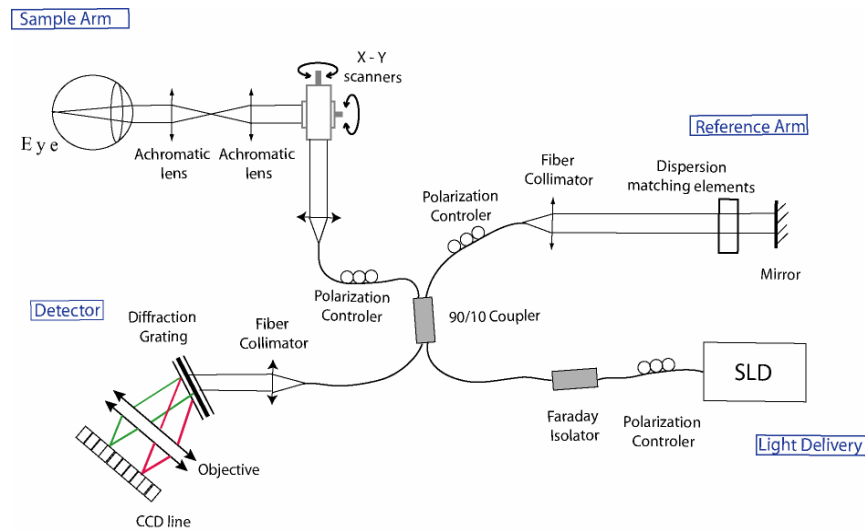

Fig. 1: Clinical Fd-OCT system at UC Davis. The reference arm matches the path length of the sample arm.

Volumetric data presented in this paper have been acquired over 6x6 mm lateral range using 200 horizontal B-scans (500 A-scans/B-scan). Thus, volumes consist of 100,000 A-scans acquired in 5.5 s with 50 μs CCD exposure time. Software from Bioptigen, Inc. was used to acquire and display the data as well as for driving both horizontal and vertical scanners. This software permits real-time display (at the acquisition speed) of the imaged retinal structures and saving of the last acquired volume (200 B-scans). Figure 2 shows the relative lateral locations of two retinal volumes used in this paper superimposed on a fundus image.
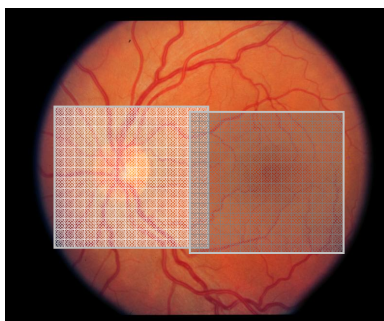
Fig. 2: The OCT scanning areas of 3D volumetric measurements used in this paper superimposed on a fundus photo.

To visualize and analyze our 3D OCT data, we post-process raw OCT data and save them as consecutive B-scans in tiff file format. This is represented on a figure 3.
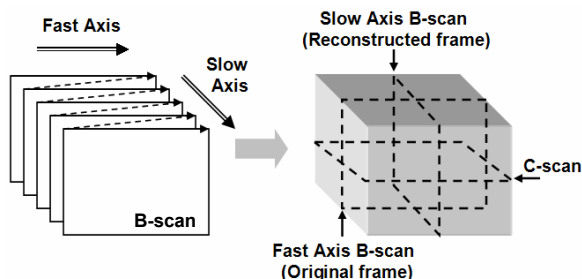

Fig. 3: The OCT scanning pattern used in volumetric acqusition (left) and its volumetric representation with virtual cutting planes (right).

In our standard volumetric imaging mode Fast Axis corresponds to horizontal scanner and Slow Axis corresponds to vertical scanner. This is later used as the input for our auto registration software as well as for our volumetric visualization software that has built -in scanning beam distortions correction algorithm. Respectively this volume can be later virtually cut along and plane allowing reconstruction of the virtual Slow Axis B-scans and C-scans.

2.2. Motion Artifacts

In Fd-OCT, head and eye motion can result in B-scans distortions as well as decreases in image intensity (due to the fringe wash out). In this paper we will concentrate only on image distortions only.

2.2.1. Head and Eye motion

In general, motion artifacts are minimized with faster image acquisition speed. Conversely, the amount of motion artifact, even though it strongly depends on the imaging subjects, increases with increasing acquisition time. In the ideal case, very fast volume acquisition speed (less then 100 ms) would allow virtually motion-free imaging. This however is still not possible in current ophthalmic OCT instruments unless the number of A-scans /Volume is reduced, but this will severely limit volumetric detail. Volumetric retinal imaging thus requires a compromise between lateral sampling density and total acquisition time. As with other ophthalmic imaging instruments, use of a chin and forehead rest or bite bar with forehead rest helps to reduce head motions and therefore lower axial motion artifacts. A fixation target (point) also helps the subject to focus and reduce voluntary eye motion artifacts. Unfortunately, these methods cannot completely remove motion artifacts and additional correction is necessary. In this paper we will simplify our motion artifact model to three degrees of freedom only. Namely we will assume that retinal image can be translated axially (along the z-axis) and laterally (along x- and y-axes). Figure 4 illustrates motion artifact distortions.
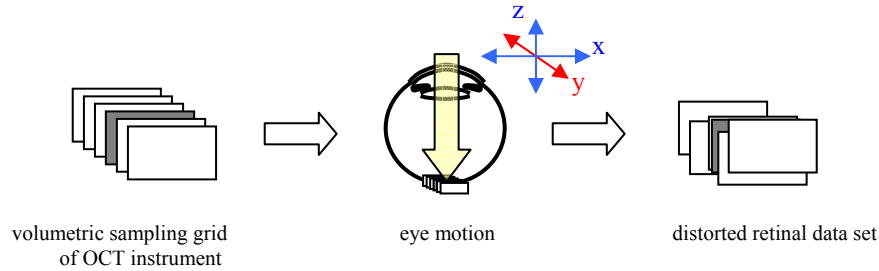
Fig. 4. Schematic of the eye and head motion caused artifact. Due to eye and head motion, the retina is sampled with a distorted sampling grid. Blue arrows indicate degrees of freedom used to correct for displacements between consecutive B-scans. Red arrow represents direction where no correction is performed.

2.2.2. Motion artifact correction

The initial motion artifact correction method presented in this paper is relatively simple and is often used in the OCT community. Here only distortions between consecutive B-scans are corrected, thus no correction on a single B-scan is performed. This method is useful for correcting slow fixation drift of the eye and some head motion on a time scale longer than a single B-scan acquisition time. Thus in this method very fast eye motions are not corrected and can be still seen on single B-scans. To correct for axial and lateral distortions between consecutive B-scans, we use an autocorrelation method that shifts (alignes) stack of frames. This was implemented with ImageJ [9] with the Turboreg plugin developed in P. Thévenaz, laboratory at Biomedical Imaging Group, Swiss Federal Institute of Technology Lausanne [10]. In their algorithm each frame is used as the template with respect to which the next frame is aligned, so that the alignment proceeds by propagation. After completion of the registration process, the original stack of frames is destroyed and replaced by the result of the registration. During testing of this algorithm we found out that distortion of the stacks with translation only bring best results. Thus upon translation, a straight line on a B-scan is mapped to a straight line of identical orientation, with conservation of the distance between any pair of points. A single landmark in each image gives a complete description of a translation. Thus each B-scan stays not distorted and we get set of B-scans corrected along Z-axis (depth) and X-axis (fast lateral axis). We find this method quite successful if amount of motion artifact is moderate. To estimate results of this correction one can view virtual C-scan or slow Axis B-scan. If no disruption can be observed on both, then motion artifact correction was successful and data can be used for further image processing.

2.2.3. Elimination of the axial flattening artifact in autocorrelation methods

It is important to point out that implementation of the B-scan correlation method may result is some loss of information about retinal structure along the slow-axis. Thus to retrieve this information one can use additional B-scans acquired along the slow axis (with vertical scanners scanning fast) and use this as a reference retinal profile for axial shifts of the consecutive B-scans to achieve an unflattened profile along the slow axis. Figure 5 shows a schematic of this operation.
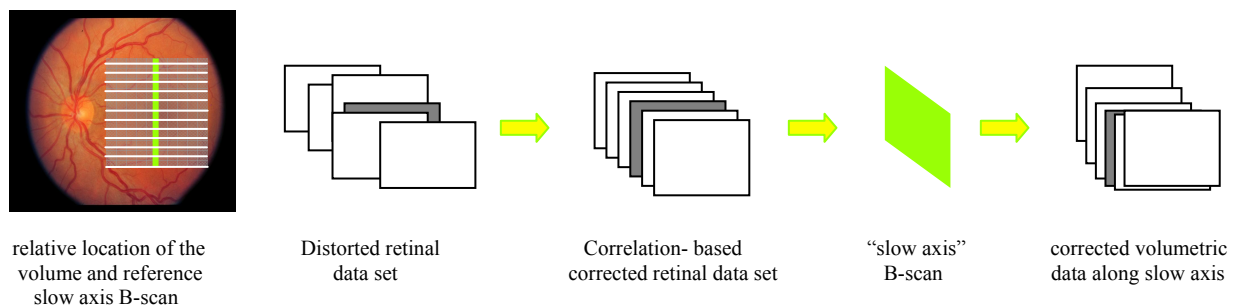

Fig. 5. Schematic of the slow-axis axial flattening artifact removal. Separate reference "slow-axis" B-scan is used to correct for axial flattening along the slow axis.

In the actual implementation of this method one needs to locate the reference slow-axis frame on the virtually reconstructed slow axis B-scans (from the volume). Then, the axial position of the A-scans from the reconstructed B-scans should be correlated with the A-scan on the reference frame. As a result, the set of axial displacements of each A-scan on the reconstructed B-scan is found. This information can be used to shift axially fast axis B-scans allowing removal of the flattening artifact.

2.3. Scanning system distortion

As with ultrasound imaging, distortions from scanning in ophthalmic OCT data acquisition (in polar coordinates), need to be taken into account for undistorted data display. Because two separate scanners are used in volumetric image acquisition, two separate image distortion corrections in two coordinate systems must be performed, first along the slow axis planes and then along the fast axis. The correction methodology presented in this paper is similar to the one proposed by Podelanu et al. [7].

2.3.1 Geometry of the scanning system and the eye

To model and later correct distortion created by the OCT scanning system, one needs to use a model of the OCT scanning head and the imaged eye. Similarly to most commercial and laboratory OCT ophthalmic systems, we used an OCT sample/scanning head consisting of a fiber collimator, two scanners (for vertical and horizontal scanning) and two lenses that image scanners onto the eye's pupil. Additional correction may be required if trial lenses are used to correct a subject's refractive error (defocus). Figure 6 presents a schematic of a standard OCT scanning system.
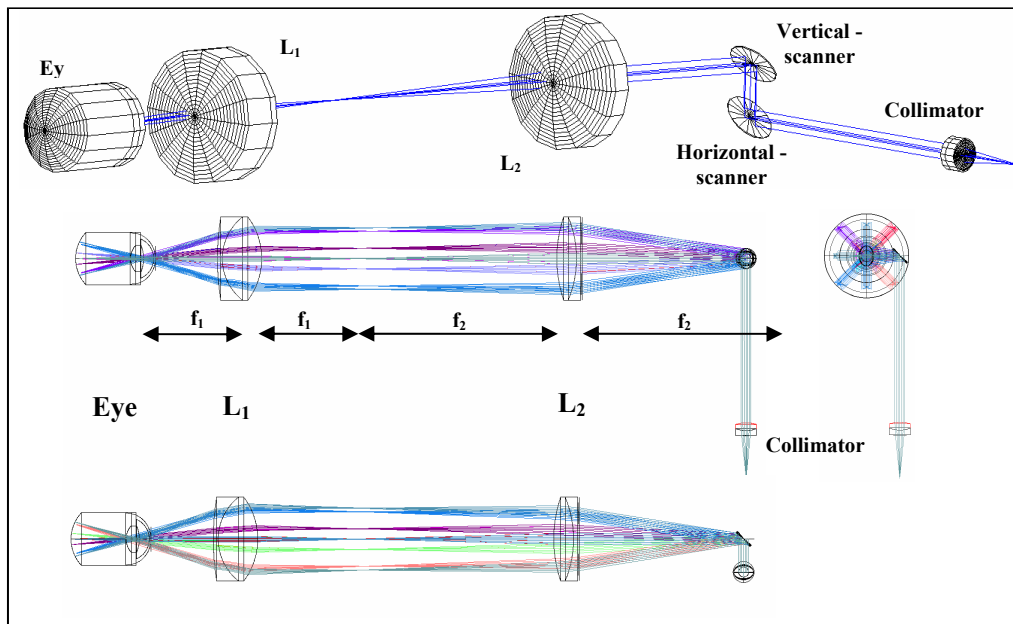

Fig. 6. Schematic of the OCT scanning head geometry. Top: 3D view simulated in ZEMAX; Bottom: 2D view of the elements; L_1 - Lens 1; L_2 - Lens 2; f_1 - focal length of Lens 1; f_2 - focal length of Lens 2;

In this standard configuration, rays are scanned from the central pivot point originating in the eye pupil. The exact position of this pivot point depends on the location of the eye with respect to the lens, L1. Due to the separation between vertical and horizontal scanners, their pivot points are separated as well, creating references for two perpendicular polar coordinate systems, one for vertical planes and one for horizontal planes. Figure 7 is a schematic of OCT scanning geometry and sampling grid density on the OCT B-scans defined by angular steps of the scanners ($\Delta\Phi$) and depth sampling (Δr) for both horizontal and vertical planes.
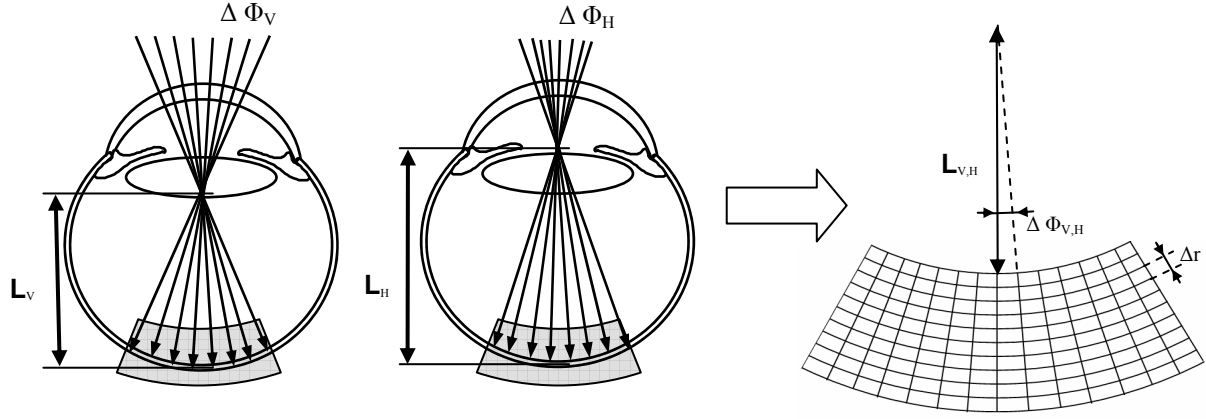
Fig. 7. Scanning geometry and sampling grid of the OCT retinal system; Left: schematic of the ray's path inside subject's eye for vertical scanning plane. Center: schematic of the ray's path inside subject's eye for horizontal scanning plane. $L_{V,H}$ distance between pivot point and retina for vertical (V) and horizontal (H) scanning pattern. Right: 2D sampling grid of the OCT system with the axial sampling (Δr) and radial sampling ($\Delta \Phi$) for vertical (V) and horizontal (H) scanning pattern.

The separation between vertical and horizontal scanners in our OCT scanning head transfer into a 4 mm separation between vertical plane and horizontal plane pivot positions. Driver signals of our scanning system have been corrected for separation of vertical and horizontal pivot points to produce undistorted lateral patterns on the retina.

2.3.2. Correction of the scanning system distortions

To properly display OCT scans on a computer screen (that relies on evenly sampled data) we need to resample our data from polar to Cartesian coordinates. In our method new equidistant points are used with intensity found by linear interpolation based on the neighbor's intensity value. We treat our original data set a three dimensional matrix S_{ijk} with the i encoding number of the A-scan along fast axis, j encoding number of A-scan along slow axis and k encoding depth location of the point.

$$S_{ijk} = S(r_{ijk}, \Theta_{H\ ijk}, \Theta_{V\ ijk}) \tag{1}$$

where:

$$i - \text{Fast axis (X); I - size}$$

$$j - \text{Slow Axis (Y); J - size}$$

$$k - \text{Depth (Z); K - size}$$

The next step uses the scanning system geometry to find locations for each point in the matrix S. This is performed in two steps. First we find points located on the-fast-axis plane and then resample it to equidistant coordinate system.

$$S_{ijk}\Big|_{Fast\ Axis\ plane} = S(r_{ijk}, \Theta_{H\ ijk})\Big|_{j=0}^{J} \overset{Interpolation}{\Rightarrow} S_{xz}\Big|_{Fast\ Axis\ plane} \tag{2}$$

where:

$$r_{ijk} = L_H + k \cdot \Delta r\Big|_{j=0}^{J}$$

$$\Theta_{H\ ijk} = \left(-\frac{I}{2} + i\right) \cdot \Delta\Theta_H\Big|_{j=0}^{J}$$

Figure 8 shows a graphical representation of this process on a single fast-axis plane. This operation is repeated for each of the fast axis B-scan planes.
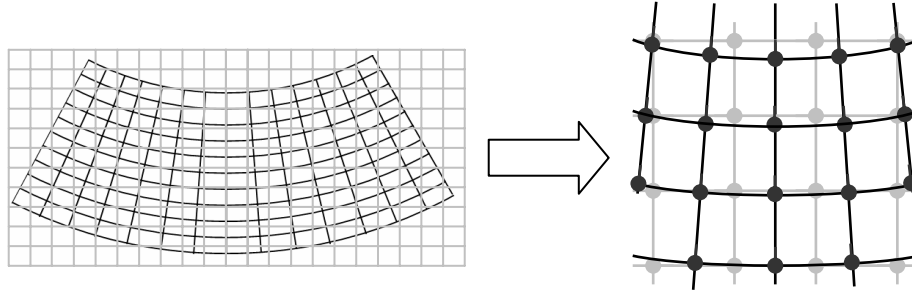

Fig. 8. Schematic of the resampling OCT data from radial to Cartesian coordinates. Left: orientation of the original (black) and resampled (grey) Field of View, Right: locations of the data points on the radial coordinates (black) and Cartesian coordinates (interpolated points that will be displayed)

The next step on this already corrected along fast-axis data set is to perform a similar operation along the slow-axis plane and then the data are again resampled into equidistant Cartesian coordinate system. This operation is performed on each slow-axis B-scan plane

$$S_{ijk}\Big|_{Slow\ Axis\ plane} = S_{xz}\Big|_{Fast\ Axis\ plane}(r_{ijk}, \Theta_{V\ ijk})\Big|_{i=0}^{I} \stackrel{Interpolation}{\Rightarrow} S_{xyz} \tag{3}$$

where:

$$r_{ijk} = L_V + k \cdot \Delta z\Big|_{i=0}^{I}$$

$$\Theta_{H\ ijk} = \left(-\frac{J}{2} + j\right) \cdot \Delta\Theta_V\Big|_{i=0}^{I}$$

Thus, by simply knowing five specific parameters of the OCT system (Δr; $\Delta\Phi_V$; $\Delta\Phi_H$; L_V; L_H), one can have a non-distorted representation of the data set in a Cartesian coordinate system I_{xyz}. The figure below shows a schematic of our scanning distortion correction algorithm.
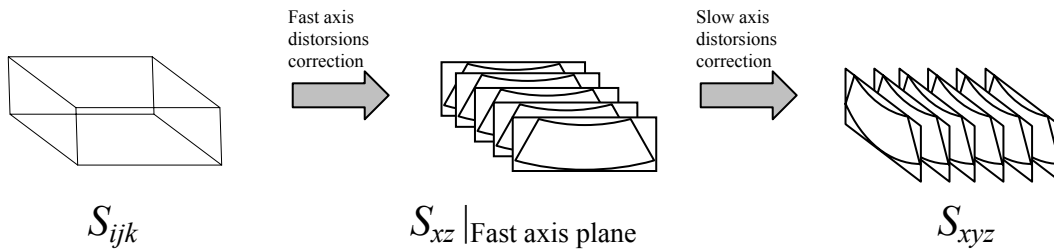

Fig. 9. Schematic of the scanning beam distortion correction. Left: original data set. Center: data set corrected for Horizontal scanner distortion; Right: data set corrected for Vertical scanner distortion.

3. RESULTS

We tested our method for reducing image distortions using two data sets acquired on the same subject's fovea and optic nerve head (ONH).

3.1. Imaging artifacts

Before presenting corrected results, we want to point out that the axial and lateral positioning of the eye' pupil in the front of the imaging lens plays a critical role in achieving good correction of the volumetric data. Any displacement of the eye along x- or y-axes will result in tilting of the retinal structures on the OCT scans. Axial displacement of the eye will result in the bending of the retinal structures seen with OCT.
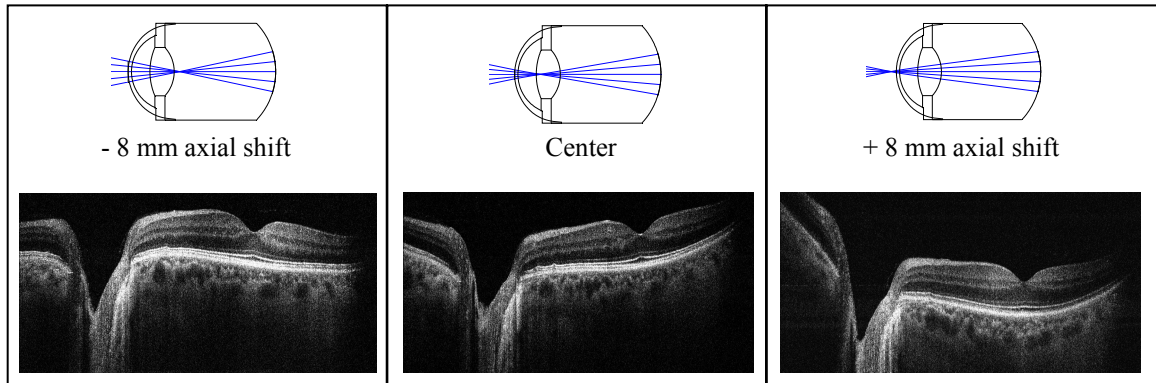

Fig. 10. Visualization of the retinal distortions caused by axial displacement of the pupil with respect to the scanning beam pivot. Top: schematic of the eye position; Bottom corresponding B-scans acquired over 12 mm. Left column represents 8 mm axial displacement toward the imaging lens; central row represents reference displacement used in our scanning beam distortion algorithm. Right: 8 mm axial displacement backwards from the imaging lens

Correct positioning of the eye's pupil is, therefore, critical for the correction method presented in this paper as it assumes central location of the pupil. This is very important because the distance between two imaging lenses is very often used to correct for subject refractive error (defocus). Thus, if one wants to keep the eye at the correct position, alteration of reference arm length is necessary. Alternatively, changes in the scanners displacement would be necessary to keep proper lateral dimensions of the scanning area on the retina. If the pupil is located off axis, a more complex distortion correction model is necessary to take into account and correct for pupil's lateral distortions.

3.2. Motion artifact correction

To illustrate the effect of eye/head motion and scanning beam distortion on the volumetric data we visualized those data without any corrections. Figure 11 shows data as acquired. Note that the axial motion artifact manifesting itself in wavy structures seen on the virtual C-scans.
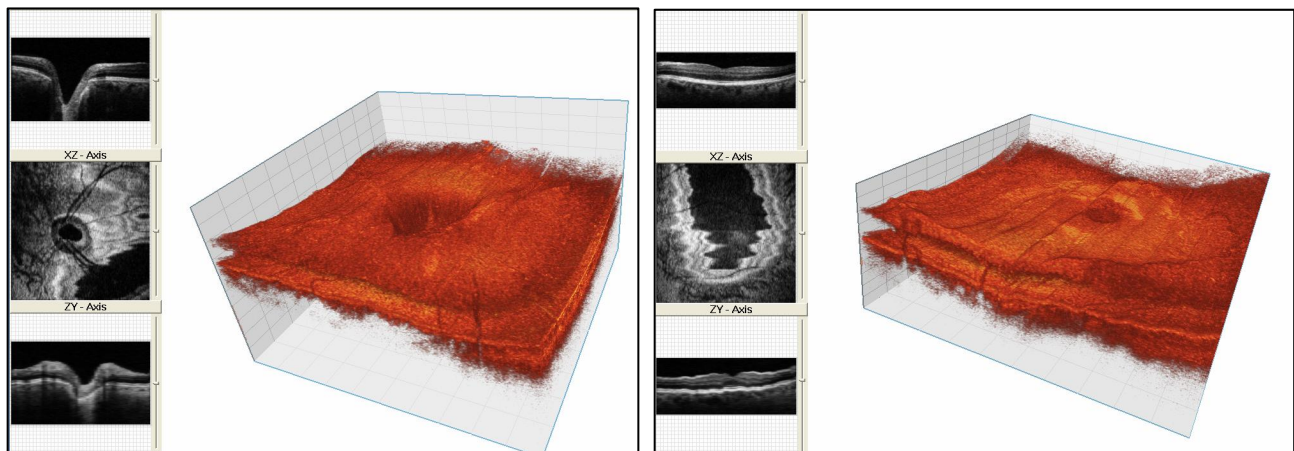

Fig.11. Visualization of "raw" volume acquired over ONH region (left) and fovea (right).

Figure 12 presents the same data after motion artifact correction. One can see that most of the wavy structures previously seen on the C-scans are now removed.
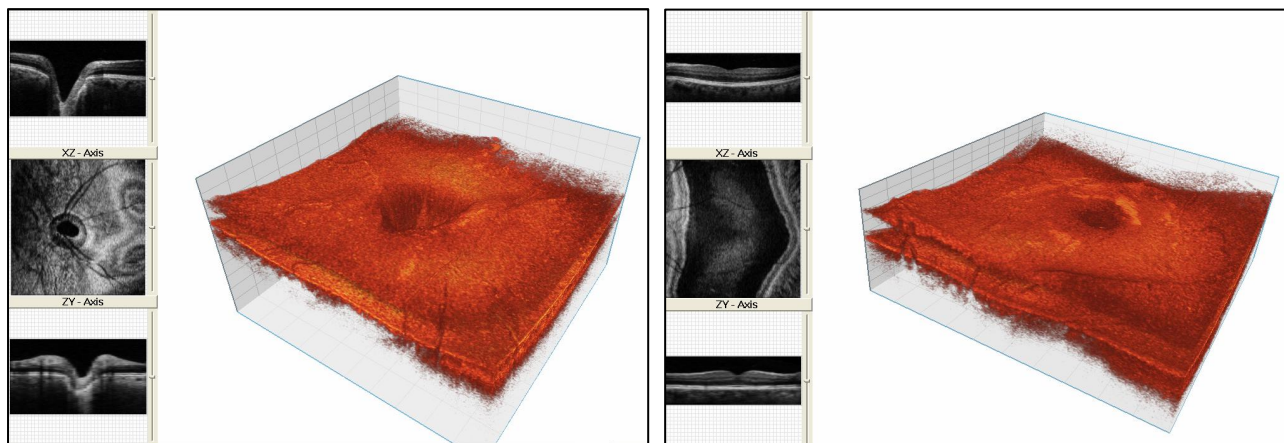

Fig. 12. Visualization of Volume acquired over ONH region (left) and fovea (right) corrected for lateral and axial motion artifacts.

3.3 Scanning beam distortion correction

In the next step, motion artifact-corrected data are used as an input for our two step scanning beam distortion algorithm. As noted, we used five parameters to perform this transformation. The axial spacing of the retinal data is $\Delta r = 0.002$ mm; the angular separation of the A-scans on vertical planes is equal to $\Delta\Phi_V = 0.0015$ rad/line; the angular separation of the A-scans on horizontal planes is equal to $\Delta\Phi_H = 0.00062$ rad/line; distance between vertical pivot pint and top of the data set is equal $L_V = 16.5$ mm, respectively; distance between horizontal pivot point and top of the data set is equal $L_H = 20.5$ mm.
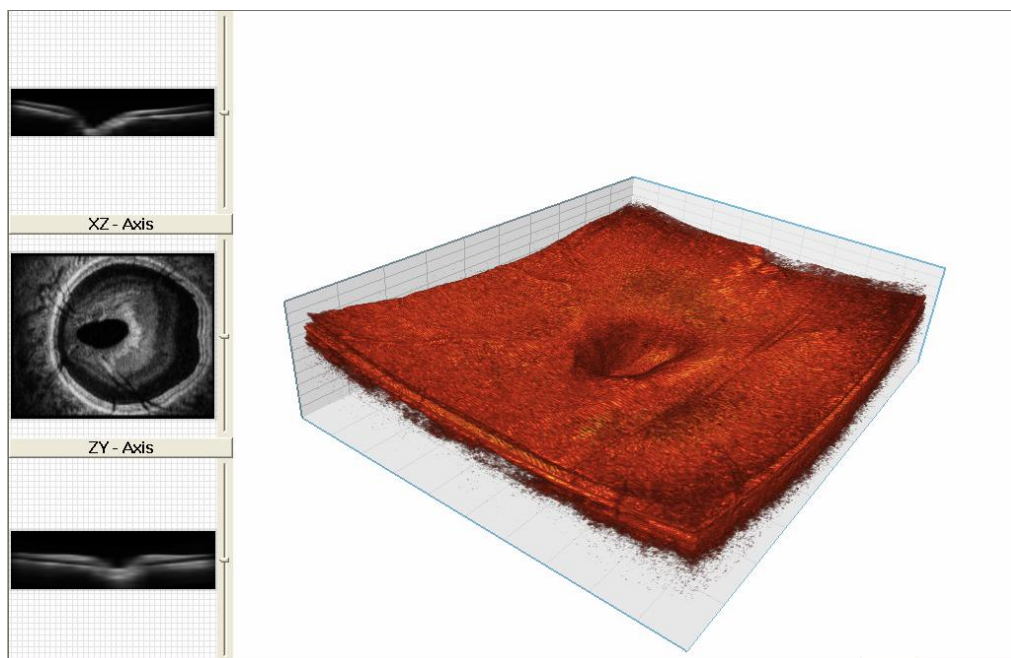

Fig. 13. Visualization of corrected volumes (along fast- and slow-axis planes) acquired over ONH region
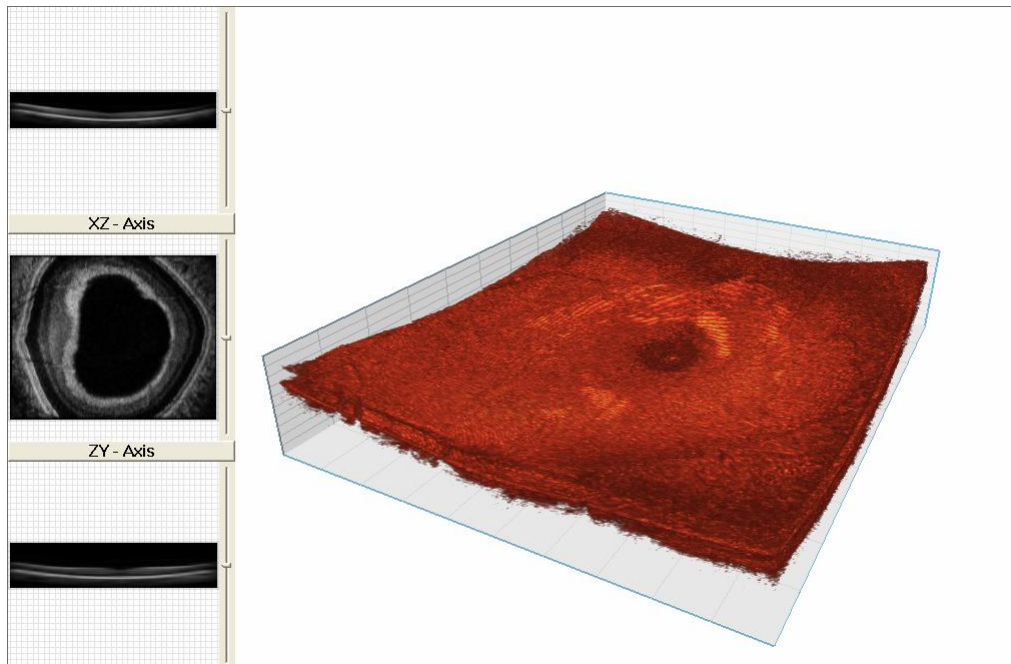
Fig. 14. Visualization of corrected volumes (along fast- and slow-axis planes) acquired over fovea.

Characteristic circular shapes seen on the reconstructed C-scans indicate the spherical shape of the retina after implementation of the scanning beam distortion correction.

4. CONCLUSIONS

A method to correct for eye and head motion and scanning beam distortion artifacts is presented. Corrected volumes show spherically shaped retinae. These results demonstrate our method in qualitative correction of retinal volumes. In order to have precisely corrected data, more accurate measurements of the correction parameters are needed. Our method could be verified with independent data acquired with other imaging techniques free of artifacts present on OCT scans. A high-resolution magnetic resonant imaging system will be used to test our method for scanning beam distortion correction.

ACKNOLEDGEMENTS

REFERENCES

1.   D. Huang, E. A. Swanson, C.P. lin, J.S. Schuman, W.g. Stinson, W. Chang, M.R. Flotte, K. Gregory, C.A. Puliafito, "Optical Coherence Tomography", Science **254**, 1178-1181 (1991)
2.   A. F. Fercher, C.K. Hitzenberger, G. Kamp, Y. Elzaiat, „ Measurment of intraocular distances by backscattering spectral interferometry", Opt. Commun. **117**, 43-48 (1995)
3.   M. Wojtkowski, T. Bajraszewski, P. Targowski and A. Kowalczyk „ Real time in vivo imaging by high-speed spectral optical coherence tomography", Opt. Lett. **28**, 1745-1747 (2003)

4.   R. Leitgeb, C.K. Hitzenberger, and A.F. Fercher "Performance of fourier domain vs. time domain optical coherence tomography", Opt. Express **11**, 889-894 (2003)
5.   N.A. Nassif, B. Cense, B.H. Park, M.C. Pierce, S.H. Yun, B.E. Bouma, G.J. Tearney, t.C. Chen, J,F. de Boer "In vivo high-resolution video-rate spectral-domain optical coherence tomography of the human retina and optic nerve", Opt. Express **12**, 367-376 (2004)
6.   V. Westphal, A.M. Rollins and S. Radhakrishnan J.A. Izatt "Correction of geometric and refractive image distorsions in optical coherence tomography applying Fermat's principle", Opt. Express **10**, 397-404 (2002)
7.   A. Podoleanu, I. Charalambous, L. Plesea, A. Dogariu and R. Rosen " Correction of distortions in optical coherence tomography imaging of the eye", Phys. Med. Biol. **49**, 1277-1294 (2004)
8.   R. Zawadzki, S. Jones, S. Olivier, M. Zhao, B. Bower, J. Izatt, S. Choi, S. Laut, and J. Werner, "Adaptive-optics optical coherence tomography for high-resolution and high-speed 3D retinal in vivo imaging," Opt. Express **13**, 8532-8546 (2005)
9.   http://rsb.info.nih.gov/ij/
10.   http://bigwww.epfl.ch/thevenaz/turboreg/